JOURNAL OF COATING TECHNOLOGY AND INNOVATION
2023, VOL. 1, ISSUE 1
https://doi.org/10.61577/jcti.2023.100004

ORIGINAL ARTICLE

Comparative corrosion study of HVOF coated Wc-10Co-4Cr, NiCrBSi and NiCr industrial waste coatings on AiSi304 stainless steel

Rishabh Kumar Chandrakar[1], Sandip Kumar Nayak[2], Sisir Mantry[2], Animesh Mandal[1] and Laxmidhar Besra[2]
[1]School of Minerals, Metallurgy and Material Engineering Indian Institute of Technology, Bhubaneswar, Odisha, India
[2] Department of Materials Chemistry, CSIR-Institute of Minerals and Materials Technology, Bhubaneswar, Odisha, India

ABSTRACT

The increasing demand for the high-velocity oxy-fuel (HVOF) thermal sprayed coated steel for boiler tube applications is the driving force behind this research work. Following the needs of the industry, the present study is aimed at understanding and comparing the corrosion resistance behavior of the WC-10Co-4Cr, NiCrBSi, and NiCrIW coating on AISI 304 stainless steel. A detailed microstructural characterization of the coatings before and after the corrosion experiment by FESEM, phase identification by XRD, and porosity determination by image analysis was performed. Corrosion behaviors of the coatings are examined by the electrochemical measurement technique after their immersion in a solution of 4 % NaCl for 1 hr, 12 hr, 36 hr, 102 hr, 200 hr, and 250 hr. Electrochemical impendence spectroscopy and Potentiodynamic polarization test results show that the porosity of the coatings and interface between unmelted particle and matrix (Formation of micro-galvanic cell) are potential sites for corrosion initiation. Electrochemical impedance spectroscopy (EIS) data indicates that the corrosion resistance of all types of coating initially decreases with increasing immersion time, but after some time corrosion resistance of the coatings again increases with increasing immersion time. This is because of the local accumulation of corrosion products in the defects hindering penetration of the electrolyte easily. Both the corrosion studies revealed that corrosion resistance of the coatings is in the following order: NiCrBSi > WC-10Co-4Cr > NiCrIW.

KEYWORDS
HVOF; WC-10Co-4Cr; NiCrBSi; NiCrIW; EIS; PDP; Corrosion

ARTICLE HISTORY
Received 3 September 2023; Revised 20 October 2023; Accepted 27 October 2023

Introduction

Many industrial parts used in power generation fail due to erosion, corrosion, and abrasion, resulting in significant financial losses. Mitigating these issues generally involves changing the substance, changing the environment, or separating the material surface from the corrosive environment. Different studies have been conducted to address corrosion issues, and it has been discovered that corrosion resistant coatings have become more important in recent years. High velocity oxy fuel (HVOF) has emerged as an innovative, advanced, and increasingly evolving thermal spray coating technique for producing dense coating at low operating temperatures. Owing to its capability to provide lower porosity (less than 1 percent), many industries have accepted HVOF for its numerous benefits, including high micro-hardness, adhesion strength, erosion-corrosion and wear resistance, durability, and cost-effectiveness with homogeneous coating. To fulfill industrial requirements materials must work under harsh conditions such as corrosion, erosion, wear, and oxidation at elevated temperatures in aggressive chemical settings in a wide range of applications [1]. Many industrial parts used in different industries like power generation plants, chemical industries, paper industries, and oil industries fail due to erosion and corrosion. Coal based power generation plants in India; corrosion is the main failure mechanism for most of the industrial parts. Corrosion and erosion are blamed for huge industrial losses in thermal power plants. The solution to this problem is either changing the material or the environment. Another solution to this problem is separating the component from the environment [1]. According to Sidhu et al., in Indian boiler tubes 54% of the total production cost is maintenance cost for replacing pipes or damaged pipes [2]. Surface modification of these components is needed to protect them from the above forms of degradation [3]. Corrosion and wear are blamed for repair costs and reduced efficiency in manufacturing due to component wear, as well as catastrophic collapse of systems resulting in significant replacement costs and lawsuits [4]. These issues can be resolved by adding a thin film of anti-oxidation and anti-wear coatings with good thermal conductivity. Coating the components' surfaces with rough and/or chemically inert compounds is one of the most effective ways to protect them. The coating material selected is determined by the conditions under which the base material's surface is exposed. High stiffness with low brittleness, low friction coefficient, excellent adhesion to the surface, low internal stresses, and chemical stability are some of the most attractive properties of such materials. From corrosion safety to wear resistance, a number of coatings are used. The primary condition is that the coating method does not degrade the mechanical properties of the substrate. Furthermore, depending on the application, surface adjustment strategies differ. Ceramics are outstanding candidates for this as their arrangement is inextricably linked to their estate [4]. Many types of coating techniques such as sputtering, electroplating, thermal spraying, diffusion, and so on are available, however,

***Correspondence:** Dr. Sandip Kumar Nayak, Department of Materials Chemistry, CSIR-Institute of Minerals and Materials Technology, Bhubaneswar, Odisha, 751013, India, e-mail: nayak.sandip200@gmail.com

the choice is based on the application. Thermal spray techniques, such as flame spraying, arc spraying, plasma spraying, and high-velocity oxy-fuel spraying etc., are more widely used as compared to other coatings because of lower cost, less environmental issues, and high production rate etc. [2]. It has been established that overlay coatings are better compared to diffusion coating for high temperature applications [3]. Dr. Max Schoop, a young Swiss scientist, patented thermal spraying in the early 1900s [3]. He noticed that the hot lead shots fired from the cannon stuck to almost every surface, which gave him the idea that if metal could be melted and projected in a spray-like way and then a surface could be made up with this substance [3]. Due to the production of thermal plasmas and the need for high-temperature and wear-resistant materials and coating systems, the technology persisted but expanded in the 1970s [5]. There are different types of thermal spraying techniques like atmospheric plasma spraying, high-velocity oxy-fuel, arc spraying, combustion flame spraying, detonation gun spraying, cold gas spraying etc. [6]. However, HVOF coatings have been recognized to be corrosion resistance coatings and are being widely used because of the very low porosity, lower decarburization, high bond strength, high hardness, lower roughness, and low metallurgical defects as compared to the other thermal spray coatings [7-9]. High bond strength, very low porosity (less than 1%), low surface roughness because of high velocity and smaller powder size, high hardness and wear resistance because of higher amount of semi-molten or unmolten particles, less residual stress as compared to other technique, low environmental effect compared to electroplating method higher density and less metallurgical defects makes HVOF popular among the other spray techniques [10].

The use of HVOF WC-based coatings to extend the lifespan of materials has been very effective, for example, in the internal sections of centrifugal pumps, which have had their lifetime increased by 600% in some situations [11]. Souza et al. studied the corrosion of WC-Co-Cr HVOF coatings in erosion-corrosion conditions and discovered that corrosion can be a dominant process [12]. The WC grains are bonded with a Co matrix the hard phases have exceptional hardness, high melting point, metallic lustre, characteristic colors, and simple crystal structures. Furthermore, the WC has high electrical and thermal conductivity, as well as good wet-ting with metallic liquids [13]. The mechanical and tribological properties of the coating are influenced by the volume fraction of WC, coating porosity, and phase composition of the carbide and matrix [14]. Many previous studies on HVOF sprayed WC-Co coating have attempted to correlate the operational conditions of the deposition process with microstructure characterization, mechanical performance, erosion, corrosion and wear, but a comprehensive understanding of this subject is still not available [15]. It was reported that WC-Co coatings suffer in the corrosive environment and corrosion resistance can be increased by adding some amount of chromium [16,17]. Passivation behavior is characterized by thin film formation, which protects the surface against any charge transfer. It was reported that chromium decreases the hardness and increases the toughness of the WC-Co coating [18]. According to Otsubo et al. corrosion resistance of NiCrBSi coating is very high because of the formation of passive film on to the surface of the coating [19]. The Ni-B-Si system, with the presence of other alloying materials, is the most commonly used Ni-based powder. The addition of chromium improves the coating's oxidation and corrosion resistance at high temperatures and raises its hardness by forming hard phases. Boron facilitates the development of hard phases by lowering the melting point. Silicon is used to improve the self-fluxing properties of the material. Carbon produces strong carbides with a high hardness, which improves the coatings' wear resistance [20]. To increase the performance of the NiCrBSi coatings metals and ceramics, such as Mo, TiN, Fe_2O_3, WC, YSZ etc. are added as reinforcing phases, which improves wear and corrosion resistance of the coatings [13,21,22].

An extensive review of the literature thus, suggests that the corrosion resistance of the steel improves by the WC-10Co-4Cr and NiCrBSi coatings, but there is no report as to which is the best coating for the corrosion prevention of steel. Hence, further research is required to understand the corrosion behavior of WC-10Co-4Cr and NiCrBSi coatings for various industrial applications. Therefore, in the present investigation organized research is conducted on studying the comparative corrosion of HVOF-coated WC-10Co-4Cr, NiCrBSi, and NiCrIW coatings on AISI 304 Stainless steel in 4% NaCl solution.

Materials and Methods

Materials

The AISI 304 stainless steel used as substrate material in the present study was procured from M/s Mishra Dhatu Nigam Ltd., Hyderabad, India. The substrate material was received in the form of a thick plate having a thickness of 5 mm. It was cut using wire EDM to a size of 60 mm×100 mm as per the requirement. The target surface of the substrate was grit blasted prior to coating to obtain a roughness of the surface having a value of Ra 4.0-5.0 µm. The coating materials used in the study are WC-10Co-4Cr, NiCrBSi, and NiCrIW. The coating materials are obtained from Metallizing Equipment Co. Pvt. Ltd., Jodhpur, India.

HVOF coating on AISI304 stainless steel

The coating depositions were done at the Institute of Mineral & Materials Technology (IMMT) Bhubaneswar. The spray equipment used was a Hipojet 2700 HVOF system designed for gaseous LPG with a pressure of 7 bar and 55-60 g/pm feeding rate. The powder was manufactured by agglomeration of the powder to a particle diameter of 10-100 micron such that the average particle size was 50 micron. SAE 304 stainless steel with the size of 60 × 100 × 4 mm was used in this work. The surface of the base metal was blasted with aluminum oxide (20 mesh) with a surface roughness of 4.0-5.0 µm. Coating thickness varies from coating to coating because of the deposition efficiency of the powders. The HVOF parameters considered for the coating are given in Table 1.

Table 1. HVOF process parameters.

HVOF process parameter	Value of Parameter
Standoff distance	50 mm
Powder feeding rate	40 g/min
Carrier gas (pressure and feeding rate)	N_2 (6 bar, 6.5)
O_2 pressure (feed rate)	10 bars (250 lpm)
No. of nozzle passes	4-5 passes
Nozzle exit area diameter	3-4 mm

https://doi.org/10.61577/jcti.2023.100004

Electrochemical impendence spectroscopy

Most of the corrosion studies by electrochemical methods like potentiodynamic polarization, and cyclic voltammetry studying electrode reactions through large perturbations on the system. Reactions occur very far from the equilibrium and we observe the response. Another strategy is to perturb the cell with a small alternating signal (AC current) and observe how the device reacts to the perturbation at a steady state. Electrochemical impendence spectroscopy produces very small perturbation on the system and observes the response of the system [23]. It is very important to know what the response of the system at equilibrium is where the system is in a steady state. It is important because we want to know how much it resists when we disturb the system from a steady state. If any system resists more it means corrosion resistance of the system is high. This response is very important for the corrosion study of the system. This technique has many advantages: (a) an experimental ability to make high-precision measurements because the response may be indefinitely steady and can therefore be averaged over a long term, (b) an ability to treat the response theoretically by linearized (or otherwise simplified) current-potential characteristics, and (c) Measurement over a wide time (or frequency) range (104s to 106s or 104Hz to 106Hz). Since EIS works close to the equilibrium, it does not require details to know about the E-I response curve over a large range of over potential [23].

EIS for coatings

Impendence measurement in the case of coated substance is very difficult because in the coatings 2 types of capacitive electrical double layer form first at the electrolyte/coating interface and second at the electrolyte/metal interface. The second interface forms due to the active pores present in the coating, electrolytes penetrate through these active pores and reach the metal surface where another capacitive double layer forms. That's why porosity in the coating plays a very important role in coatings and different types of RC circuits used for modeling the EIS of coating. The equivalent circuit was originally proposed by Saenger, et al. and also used by some other coating studies [4,24]. The porosity of the coatings is also the torturous path for electrolytes which resists the flow of current. In the proposed RC circuit, RPo stands for porosity resistance and RS for the polarization resistance of the substrate. Therefore, if the porosity resistance of the coating is high, it also increases the corrosion resistance of the coatings [25]. Figure 1 presents the RC circuit for coating.

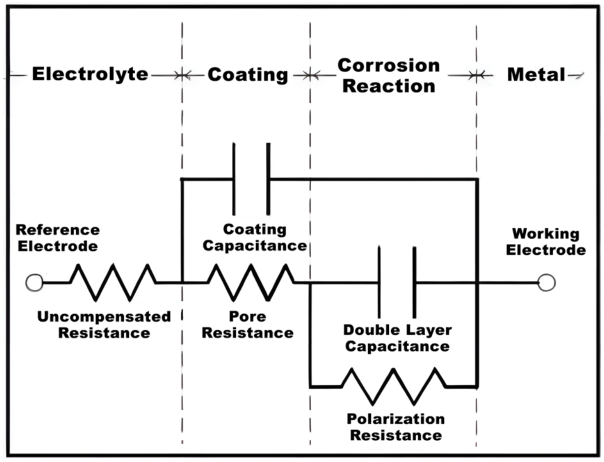

Figure 1. RC circuit for coating [24].

Experimental details of the corrosion study

The corrosion behavior of the coatings was evaluated by electrochemical measurement in a Perkin-Elmer flat cell model K0235. The practical design of the cell makes it very easy to handle and accommodate any shape of the electrode. Another advantage of this model is that it does not require dipping the entire surface of the sample into an electrolyte. Only one surface of the sample is in contact with the electrolyte. All the analyses are done by NOVA 1.11 software. Before and after the test, samples are cleaned in distilled water then acetone in an ultrasonic bath and dried in warm air. The area exposed for electrochemical measurement is 24 mm2 in 4% NaCl aqueous solutions. Three electrodes are used for the experiment, with a specimen electrode, and a platinum counter electrode and an Ag/AgCl electrode as a reference electrode. Two types of electrochemical tests are carried out to compare the corrosion behaviors of the HVOF coatings. Namely potentiodynamic polarization test and electrochemical impendence spectroscopy (EIS). The tests commenced after 100 minutes of open circuit potential stabilization. After OCP stabilization electrochemical impendence spectroscopy test was measured at the OCP with a sinusoidal potential excitation of 5mV amplitude over a frequency range of 100kHz to 10kHz. The corrosion of the coated samples was evaluated after immersion in a solution for 0 hr, 12 hr, 24 hr, 36 hr, 102 hr, 200 hr, and 250 hr. The final equivalent circuit for the electrochemical response was simulated using Autolab NOVA software. A potentiodynamic polarization test was conducted in the potential range of -500mV to +500mV (with reference to OCP) with a potential sweep rate of 1mV/s. The corrosion current density (i_{corr}) and corrosion potential (E_{corr}) were obtained by the intersection point of the taffel extrapolated anodic and cathodic curve by Origin software. The porosity of the coating was measured by area analysis of FESEM images by Image j analyzer at the magnification of 4.5kx. For accurate measurement of porosity average of the 5 images was taken for each coating shown in Tables 2 and 3. The thickness of the coatings is also measured by FESEM images.

Table 2. Elements present in NiCrIW coating.

Element	Weight%	Atomic%
B K	2.84	6.10
C K	17.54	33.94
O K	24.85	36.09
Si K	2.42	2.00
S K	0.27	0.19
Cr K	13.59	6.07
Fe K	24.67	10.27
Ni K	13.30	5.26
W M	0.51	0.06
Totals	100	

Table 3. Thickness and porosity of the coatings.

Sample	Porosity	Thickness (μm)
WC-10Co-4Cr	1.754	122
NiCrBSi	2.36	77.8
NiCrIW	1.125	56.64

https://doi.org/10.61577/jcti.2023.100004

Results and Discussion

Phase identification

XRD spectrum shows strong picks of WC with the minor picks of W_2O. The presence of W_2O indicates the decarburization of the WC. The key process that happens during thermal spraying is the decomposition of WC particles. Excessive temperatures during deposition can induce substantial decomposition or decarburization of WC particles, resulting in the formation of W_2O, η-CoxWyCz (Co_6W_6C and Co_3W_3C), dissolution of metallic tungsten and carbon in the binder phase, and the formation of an amorphous Co phase due to rapid solidification during impact [26]. Decarburization of WC is also reported to affect the mechanical and tribological behavior of the coating [26]. The hardness of the coating increases mainly because of the WC hard phase. The XRD spectrum clearly shows WC as the major phase and very less amount of other phases (Figures 2-4). This is because of the high velocity and low particle temperature. The erosion resistance of the coated sample is high as compared to the base material because of the presence of a higher amount of hard WC particles.

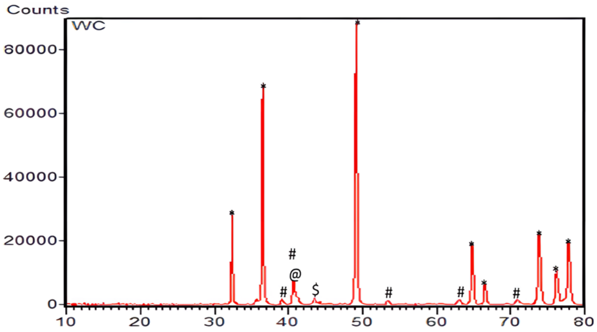

Figure 2. XRD spectrum of the WC-10C0-4Cr coating on AISI304 stainless steel. *, #, @, $ represents WC, W_2O, Co_6W_6C, $Co_3W_9C_4$ phases respectively.

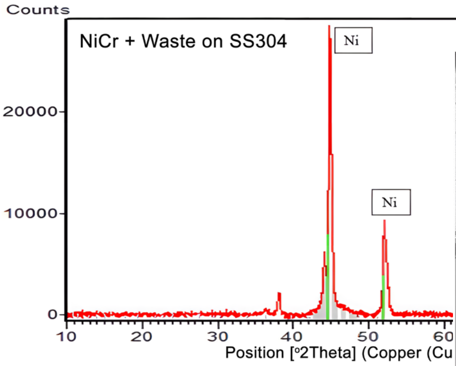

Figure 4. XRD spectrum of the NiCrIW coating on steel.

XRD spectrum NiCrBSi shows it is the amorphous structure because of the pick broadening with some Ni phase (Microstructure, wear and corrosion behaviors of plasma sprayed NiCrBSi-Zr coating) reported that the broadening of γ-Ni peaks demonstrates the existence of supersaturated solid solution. Cr, B and Si picks are absent. The amorphous structure of the NiCrBSi coating has been observed may be due to the high melting point (1025°C) of the powder [27], the high combustion temperature of the HVOF and the very high cooling rate. The melting point decreases because of the presence of the B [2]. XRD spectrum NiCrIW coating shows it is a crystalline structure. The majority of the Ni phase and some pikes of Cr.

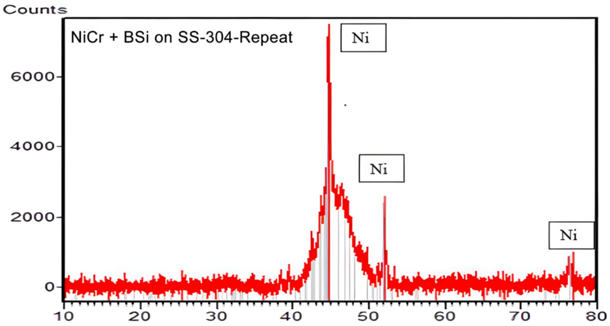

Figure 3. XRD spectrum of the NiCrBSi coating on AISI304 stainless steel.

Scanning electron microscopy

In FESEM morphology there are lots of semi molten WC particles (globular shape, bright phase), matrix (dark grey) and porosity black spots. It was observed that there are very low amount of porosity and a higher amount of WC particles. The presence of WC particles increases the hardness and tribological properties of the coating. Porosities are not completely interconnected and it is not very easy to penetrate the path for electrolytes (Figures 5 and 6).

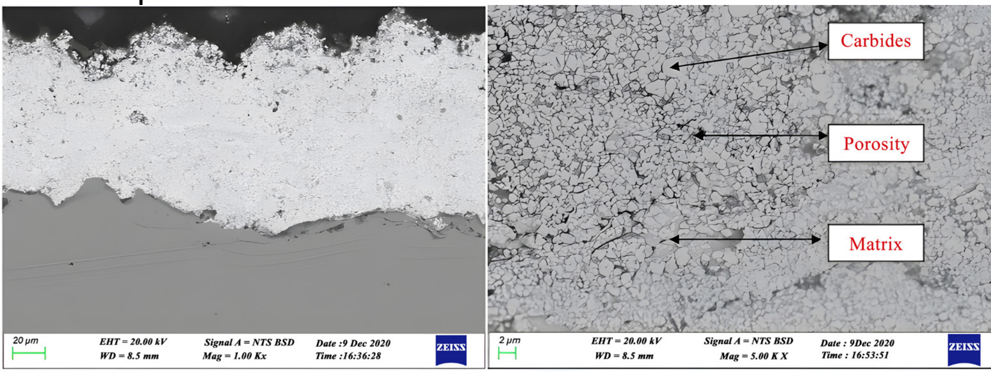

Figure 5. FESEM microstructure of WC-10Co-4Cr coating.

https://doi.org/10.61577/jcti.2023.100004

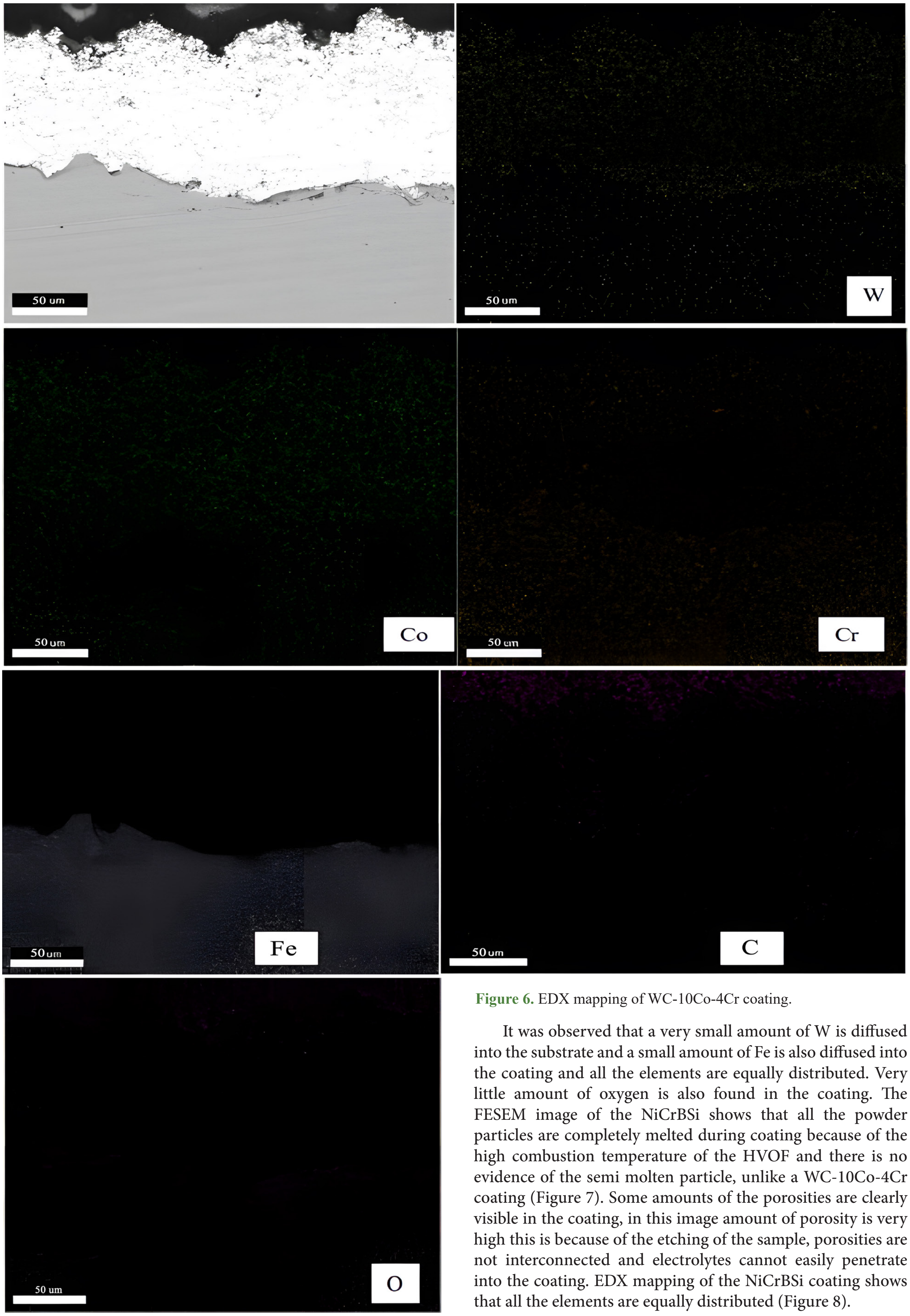

Figure 6. EDX mapping of WC-10Co-4Cr coating.

It was observed that a very small amount of W is diffused into the substrate and a small amount of Fe is also diffused into the coating and all the elements are equally distributed. Very little amount of oxygen is also found in the coating. The FESEM image of the NiCrBSi shows that all the powder particles are completely melted during coating because of the high combustion temperature of the HVOF and there is no evidence of the semi molten particle, unlike a WC-10Co-4Cr coating (Figure 7). Some amounts of the porosities are clearly visible in the coating, in this image amount of porosity is very high this is because of the etching of the sample, porosities are not interconnected and electrolytes cannot easily penetrate into the coating. EDX mapping of the NiCrBSi coating shows that all the elements are equally distributed (Figure 8).

https://doi.org/10.61577/jcti.2023.100004

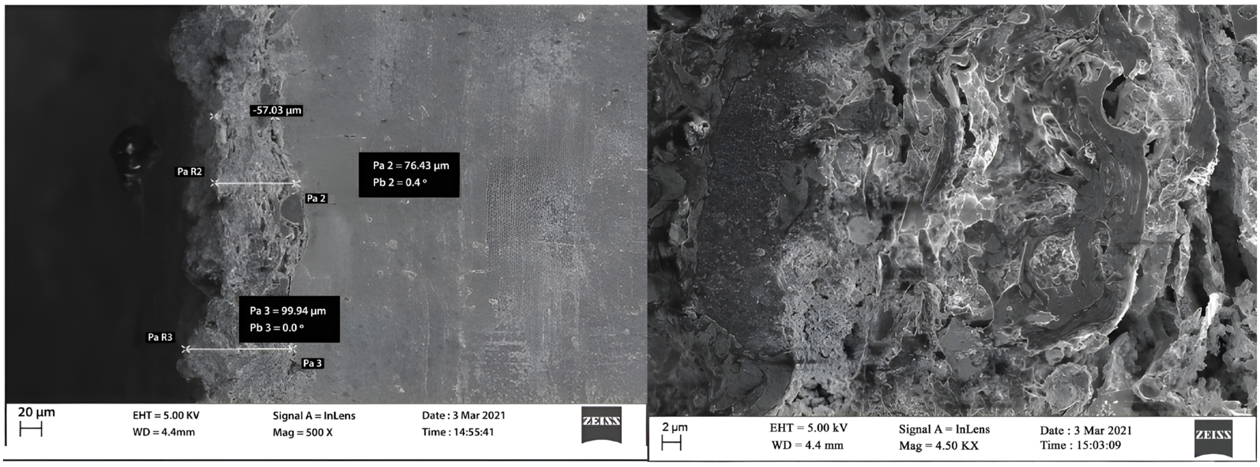

Figure 7. FESEM microstructure of NiCrBSi coating.

B Ka1_2

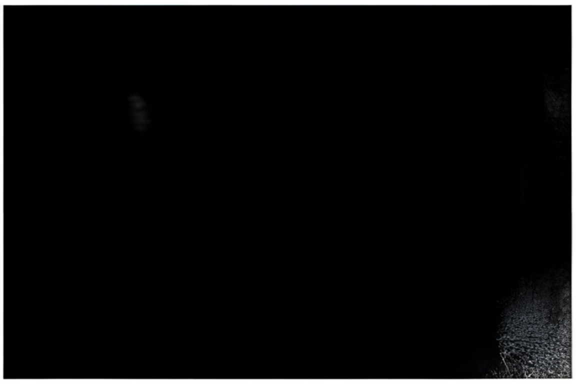

Fe Ka1

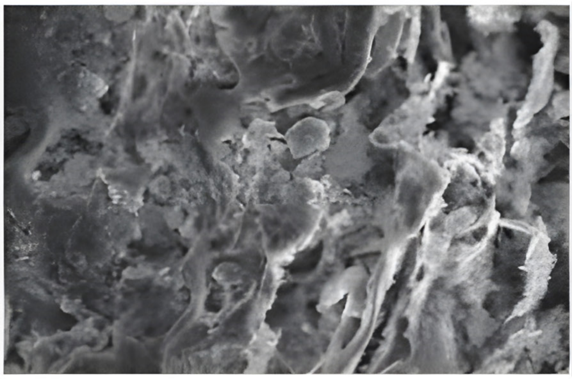

Electron Image 1

C Ka1_2

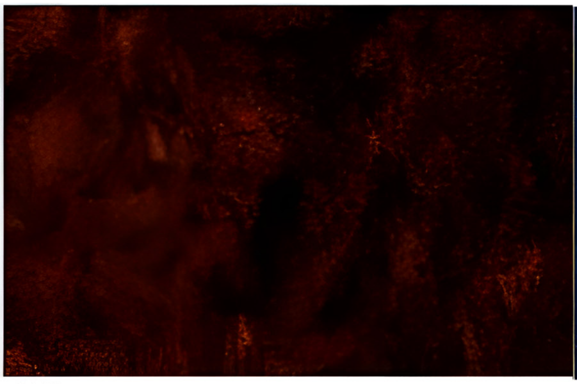

Si Ka1

Cr Ka1

https://doi.org/10.61577/jcti.2023.100004

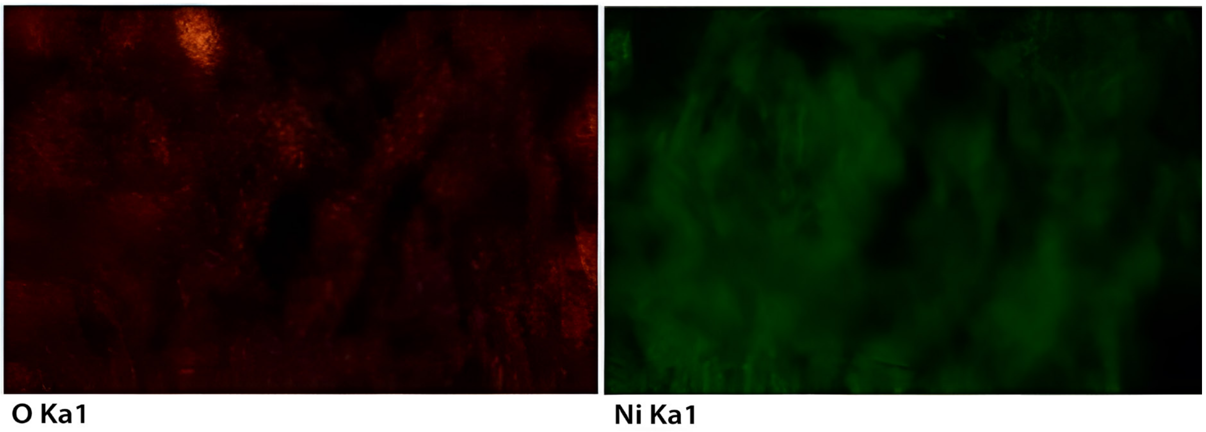

Figure 8. EDX mapping of the NiCrBSi coating.

The FESEM image of the NiCrIW shows that all the powder particles are not completely melted during coating because of the low combustion temperature of the HVOF as compared to the melting point of the NiCrIW and observing a large amount of the semi molten particles in the microstructure (Figure 9). Some amounts of the porosities are clearly visible in the coating it is also observed that the porosities of the coatings are interconnected we are saying interconnected an easier path for electrolytes because this is crossection image. It was also observed that the thickness of the coating is much less as compared to the others. EDX mapping of the NiCrIW show all the elements are equally distributed, but some amount of oxides are formed on the surface of the base metal (AISI 304 SS) called transition zone which is shown in Figure 10.

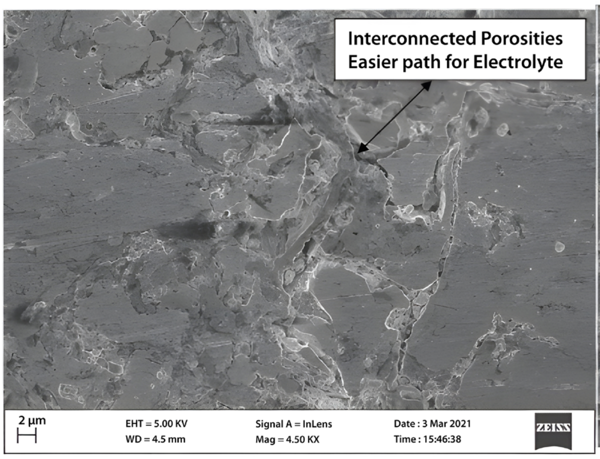

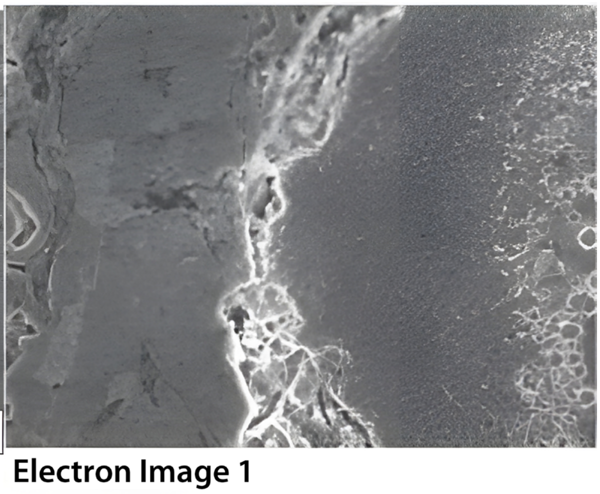

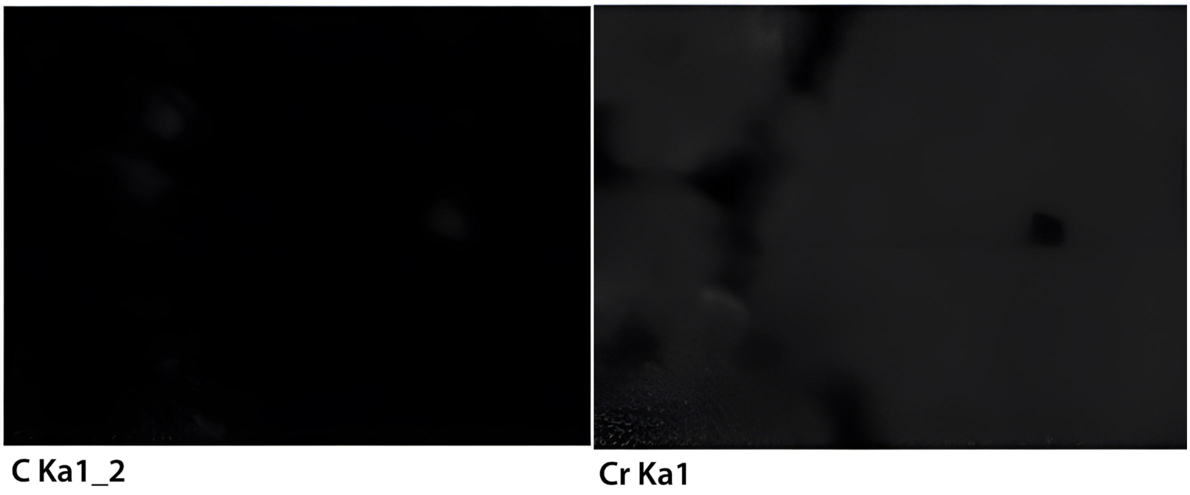

https://doi.org/10.61577/jcti.2023.100004

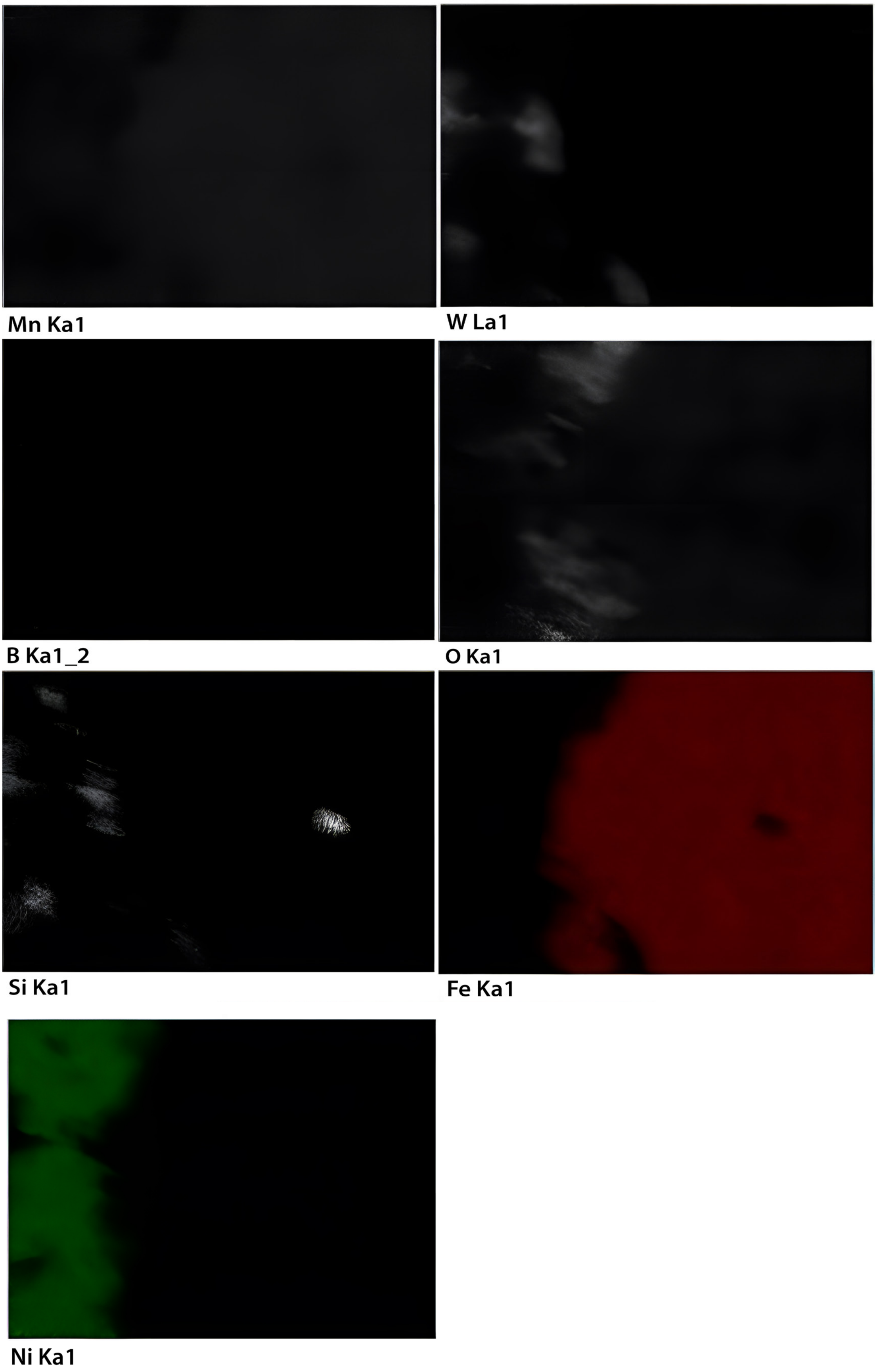

Figure 9. FESEM microstructure and EDX mapping of the NiCrIW coating.

https://doi.org/10.61577/jcti.2023.100004

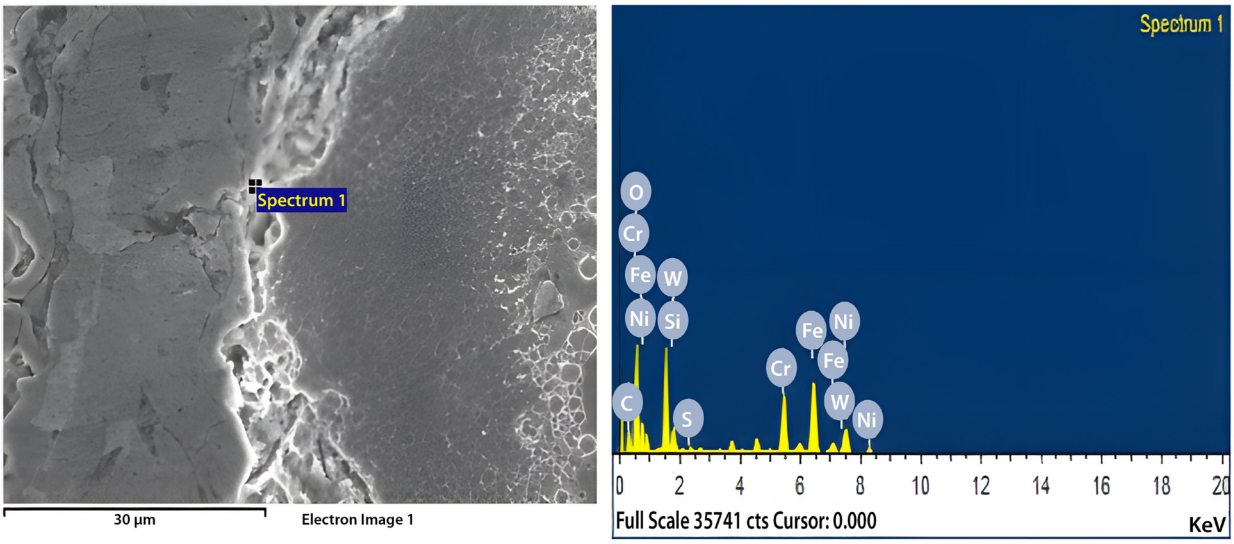

Figure 10. Point analysis of the NiCrIW coating.

Corrosion study by electrochemical impendence spectroscopy

Electrochemical impendence spectroscopy is very effective in studying the kinetics of the porous electrodes and the corrosion behavior of the coatings [4,17,25]. The corrosion resistance of the coatings depends upon the amount of porosity. If the coating has very low porosity corrosion resistance of the coating is very high [25]. Also the corrosion resistance of the coating increases if the porosities are not interconnected. The corrosion resistance of the coatings depends upon the porosity because this is the only pathway for the electrolyte. If the amount of porosity is very high, then electrolytes can easily penetrate into the coatings and corrosion resistance decreases. There are two types of coatings: (a) Coatings having active pores; which mean the wall of the porosity reacts with the electrolyte, (b) Coatings heave inactive pores, in which the wall of the porosity does not react with the electrolyte [4]. All of the 3 coating which is used in this experiment is coming under the category of the active pore. In this study for all the coatings EIS data were taken after 0 hr, 12 hr, 36 hr, 102 hr, 200 hr and 250 hr of immersion into the electrolyte (4% NaCl). The typical Nyquist (also called complex plane EIS data) and Bode plots were measured for WC-10Co-4Cr, NiCrBSi, and NiCrIW after immersion in 4% NaCl solution 0 to 250 hr are shown below. To report the effect of increasing the immersion time to 0 to 250 yr, the EIS measurements were obtained for WC-10Co-4Cr, NiCrBSi, and NiCrIW are depicted in the figure below. All the EIS data were analyzed and fitted into the circuit model that is represented in the figure. All the fitted data of impendence are listed in Tables 4 and 5. These parameters can be defined as follows: R_e is the electrolyte resistance also called solution resistance; R_s is the polarization resistance also called charge transfer resistance, R_{po} is the pore resistance, C_i and C_d are the capacitance of the coatings and double layer, respectively. Experimental data were fitted into the circuit model because 2 types of capacitive electrical double layer form first at the electrolyte/coating interface and second at the electrolyte/metal interface. The second interface forms due to the active pores present in the coating. The electrolyte penetrates through these active pores and reaches the metal surface at which another capacitive double layer forms. Some part of the current takes part in the reaction (corrosion) and can be modeled by a parallel capacitor/resistor combination. In this experiment, we used two circuits for fitting the EIS data. When we observe only one capacitive loop in the Nyquist plot and one inflection point on the corresponding bodes phase, it implies that the coating is very dense and can form a passive layer. This indicates that corrosion has not been initiated and this electrochemical cell can be modeled by a simple equivalent circuit as shown in Figure 11. When we observe two capacitive loops in the Nyquist plot and two inflection points corresponding bodes phase. It implies that the coating is not very dense (porous) and can form a passive layer, but electrolytes reach the coating/base metal interface and corrosion starts. This electrochemical cell can be modelled by a complex equivalent circuit which is shown in Figure 12.

Table 4. Fitting data for the WC-10Co-4Cr coating.

Sample	R_e ohm (cm^2)	R_{po} ohm (cm^2)	γ_1	N	R_s ohm (cm^2)	γ_2	N	OCP
WC-0h	4.25	6633.8	0.000115	0.56	-	-	-	-0.098
WC-12h	6.57	5515.44	0.000551	0.55334	-	-	-	-0.134
WC-36h	6.77	100	0.004	0.49	6346.8	0.00033	0.623	-0.126
WC-102h	6.288	1274.41	0.00057	0.4854	8026.4	0.000233	0.619	-0.094
WC-200h	10.338	1100	0.0018	0.46	1717.92	0.001	0.83	-0.127
WC-250h	4.76	1547	0.00028	0.55	26400	0.00022	0.31	-0.074

https://doi.org/10.61577/jcti.2023.100004

Table 5. Fitting data for the NiCrBSi coating.

Sample	R_e	R_{po}	γ_1	N_1	R_s	γ_2	N_2	OCP
BSi-0h	17.30	86256	0.0003	0.65	-	-	-	-0.128
BSi-12h	20.81	16348.8	0.0001	0.62	-	-	-	-0.268
BSi-36h	14.76	9649	0.0002	0.61	-	-	-	-0.280
BSi-102h	18.48	16453.7	0.001	0.62	-	-	-	-0.300
BSi-200h	15.312	6472.8	0.0003	0.6627	-	-	-	-0.303
BSi-250h	7.2	2.7.74	0.00011	0.63	6640.8	0.000145	0.74	-0.316

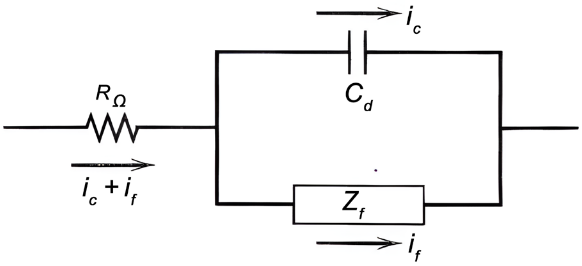

Figure 11. RC circuit for the coating [28].

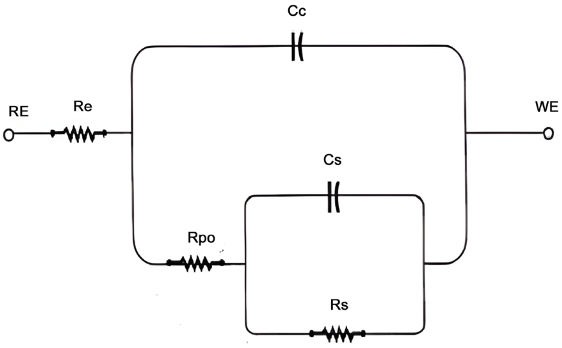

Figure 12. RC circuit for the coatings [4].

In general, the polarisation resistance (R_p) is inversely proportional to the length of the chord of the expanded semicircle when it intersects the real (horizontal) axis [29]. It means if the diameter of the semicircle in the Nyquist plot decreases, the corrosion resistance of the coating decreases. For the WC-10Co-4Cr coating the increased exposure time resulted in a decreased diameter of the semicircle, which means the corrosion resistance of the coating decreases when the exposure time increases (Figure 13). This is most likely due to the accelerated corrosion attack on the steel surface caused by chloride species [17]. Figures 13 and 14 show the Nyquist and bode plots of the HVOF coated WC-10Co_4Cr coating at various immersion times, respectively. One capacitive loop can be seen on the Nyquist plot (Figure 13) after 0 hr and 12 hr of exposure, as well as one inflection point on the corresponding bode phase diagram (Figure 14). It denotes that the system has only one time constant. The coating characteristics can be physically related to the high-frequency loop [30]. A simple equivalent circuit can be used to model this electrochemical cell. This means the corrosion resistance of the coating decreases with increasing exposure time, because the diameter of the semicircle decreases, but the base metal is still free from corrosion.

However, there is evidence of the formation of a small initial semicircle at 36 hours, signaling the start of corrosion. We observe two capacitive loops in the Nyquist plot (not clearly visible) and two inflection points on the corresponding bode phase (clearly visible). This phenomenon was also observed after 102 hr, 200 hr, and 250 hr, but the difference is after 250 hr the immersion diameter of the small initial semicircle increases.

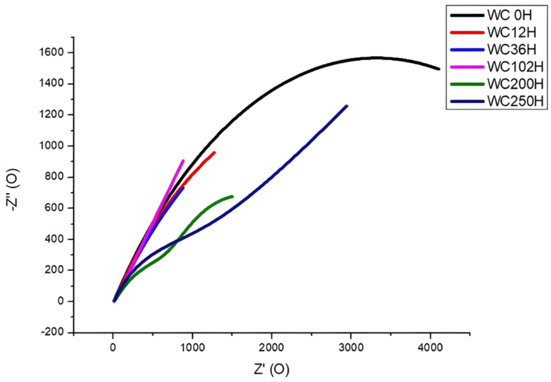

Figure 13. Nyquist plot for the WC-10Co-4Cr coating (Z(O) = ohm.cm^2).

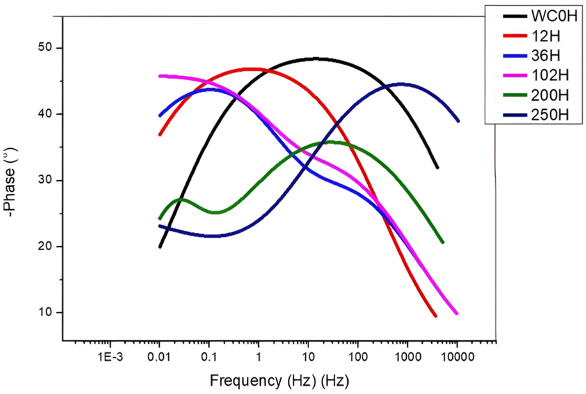

Figure 14. Bode plot for the WC-10Co-4Cr coating.

https://doi.org/10.61577/jcti.2023.100004

This is because of the local accumulation of corrosion products in the defects that hindered penetration of the electrolyte, resulting in an increase in pore resistance [3]. OCP value increases from -0.127 to -0.074 V and the 2nd capacitive loop also increases after 250 hr of immersion, which is most probably because of the local accumulation of corrosion product at the coating/substrate interface.

In this experiment also the OCP value decreases from -0.098 to -0.134 V and pore resistance decreases with increasing immersion time (0 to 12 hr). But after 36 hr, the OCP value again increased from -0.134 to -0.126V and the total resistance (solution+pore+polarization) also increased, which indicates that the corrosion resistance of the coating increased. The corrosion resistance of the coating further increases till 102 hr because OCP value again increases from -0.126 to -0.094V which is most probably because of the accumulation of corrosion products near the defects. This is because the pore resistance of the coating increases. But after 200 hr, corrosion resistance again decreases because the OCP value decreases from -0.094 to 0.127V which is most probably because WC particles act as a cathode and CoCr matrix act as an anode and forms a small micro-galvanic cell. The formation of micro-galvanic cells and dissolution of the CoCr matrix results in the removal of the WC particles from the coating which again makes a path for the penetration of electrolyte. After 36 hr the EIS data were fitted into the complex equivalent circuit because all the data shows 2 times constant in the bode phase plot, indicating that the HVOF coated WC-10Co-4Cr coating shows very complex corrosion behavior.

Figures 15 and 16 show the Nyquist and bode plots of the HVOF-coated NiCrBSi coating at various immersion times, respectively. One capacitive loop can be seen on the Nyquist plot (Figure 15) after 200 hr of exposure, as well as one inflection point on the corresponding bode phase diagram (Figure 16). It denotes that the system has only one time constant. The coating characteristics can be physically related to the high frequency loop [3,30]. A simple equivalent circuit can be used to model this electrochemical cell. This means the corrosion resistance of the coating decreases with increasing exposure time, because the diameter of the semicircle decreases, but the base metal is still free from corrosion. The OCP value decreases with increasing immersion time (0 to 200 hr) from -0.128 to -0.303 and resistance also decreases from 862556 to 6472.8 Ω. This also indicates the same.

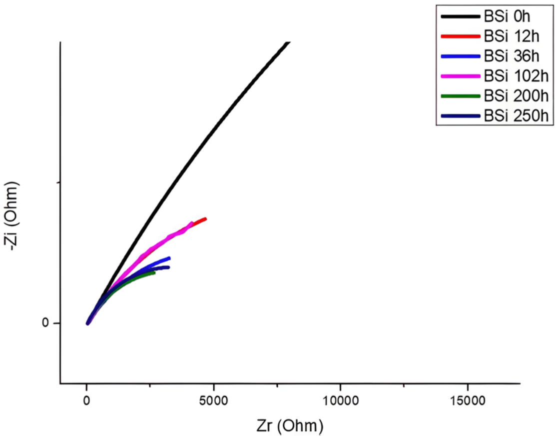

Figure 15. Nyquist plot for the NiCrBSi coating (Z(O)=ohm.cm²).

However, there is evidence of the formation of a small semicircle at 250 hr, signaling the start of corrosion. We observe two capacitive loops in the Nyquist plot (not clearly visible) and two inflection points corresponding bode phase (clearly visible). This indicates that for NiCrBSi coating corrosion starts much later after 200 hr, as compared to the WC-10Co-4Cr coating (in which corrosion starts after 12 hr). This indicates that NiCrBSi coatings exhibit higher corrosion resistance and last longer without corrosion than the WC-10Co-4Cr coating.

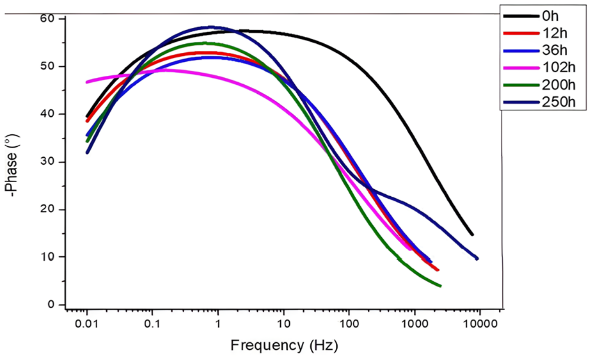

Figure 16. Bode plot for the NiCrBSi coating.

Figures 17 and 18 show the Nyquist and bode plots of the HVOF-coated NiCrIW coating at various immersion times, respectively. For NiCrIW coating initially, we observe two capacitive loops in the Nyquist plot (not clearly visible) and two inflection points corresponding bode phase (clearly visible). This indicates that the corrosion resistance of the NiCrIW is very low compared to NiCrBSi and WC-10Co-4Cr coatings (Table 6). This is probably because in the case of NiCrIW coatings porosities are interconnected which is clearly visible in the FESEM image shown in Figure 19.

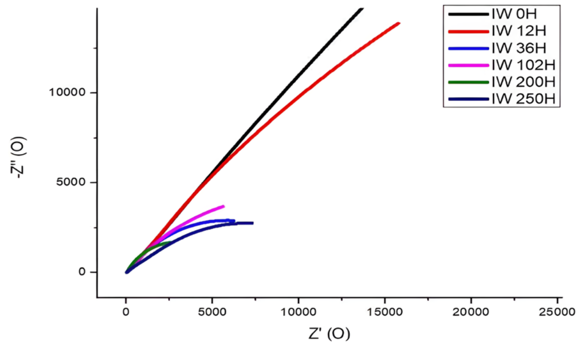

Figure 17. Nyquist plot for the NiCrBIW coating (Z(O) = ohm. cm²).

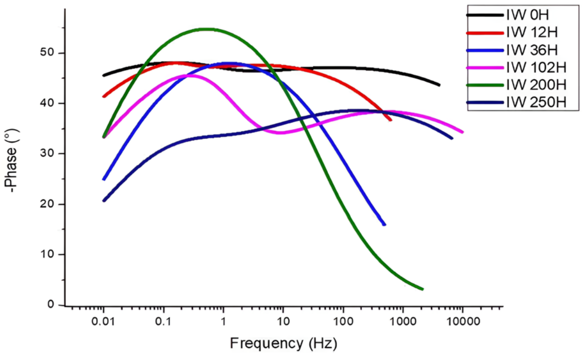

Figure 18. Nyquist plot for the NiCrIW coating.

https://doi.org/10.61577/jcti.2023.100004

Table 6. Fitting data for the NiCrBIW coating.

Sample	R_e	R_{po}	γ_1	N_1	R_s	γ_2	N_2	OCP
IW-0h	4.43	21402.24	0.00002	0.53	408000	0.00002	75	-0.125
IW-12h	6.07	41520	0.00004	0.55	66720	0.00005	0.97	-0.140
IW-36h	25.23	11523.36	0.00009	0.59	-	-	-	-0.254
IW-102h	3.43	993.432	0.00008	0.47	20385	0.00003	0.82	-0.317
IW-200h	19.41	5878.2	0.00032	0.67	-	-	-	-0.249
IW-250h	10.53	3387.6	0.000042	0.47	10231.2	0.00003	0.57	-0.320

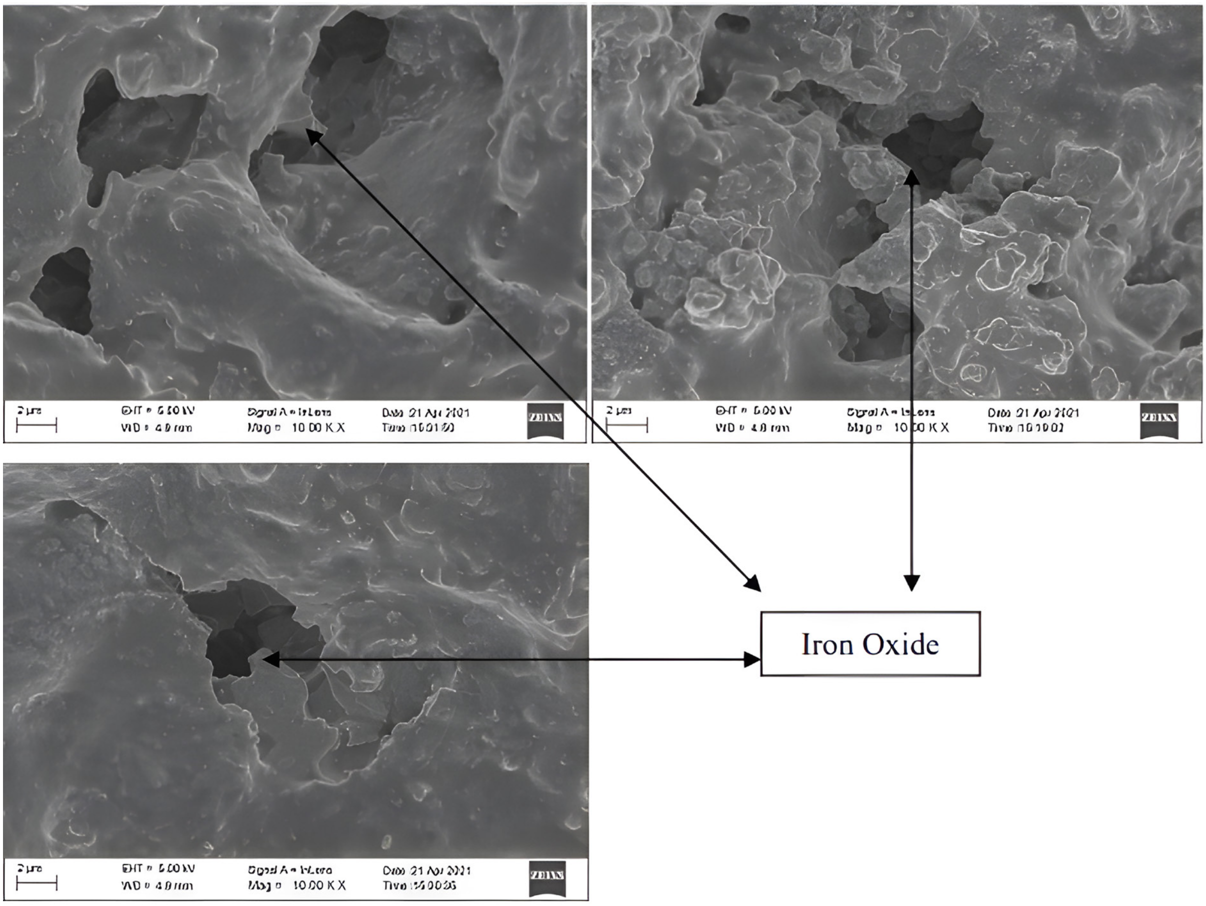

Figure 19. FESEM image of the NiCrIW, WC-10Co-4Cr, and NiCrBSi coatings respectively, after 250 hr of immersion in 3.5% NaCl solution.

Corrosion starts just after immersion and resistance of the coating to corrosion decreases with increasing exposure time which is also evident by the decrease in diameter of the semicircle with exposure time. But in the case of 36 hr and 200 hr corrosion resistance of the coating again increases and it shows only one capacitive loop which indicates that the electrolyte cannot be able to penetrate through the pores. This is probably because of the accumulation of corrosion products near the defects. The increase in OCP value from -0.317V for 102 hr to 0.249V for 200 hr indicates corrosion resistance increases but not observes after 12hr where corrosion resistance again increases and the corrosion behavior of the NiCrIW is very complicated. But the Υ value of the NiCrIW is very low as compared to NiCrBSi and WC-10Co-4Cr, this again indicates that the corrosion resistance of the NiCrIW coating is low as compared to NiCrBSi and WC-10Co-4Cr coatings.

The FESEM micrograph forms the surface of coatings after 250 hr of immersion in the electrolyte are shown in Figure 19. The surface pores can be observed in this figure, corrosion products form inside the pores, and EDX analysis shows that it contains iron and oxygen. It shows that corrosion products are formed and block the pore.

https://doi.org/10.61577/jcti.2023.100004

Corrosion study by potentiodynamic polarization test (PDP)

The potentiodynamic polarization test (PDP) was conducted after 250 hr of immersion over the potential range of -500 to + 500V with reference to OCP value and the scan rate was chosen 1 mVs-1. The passivation behavior of all types of coated samples was studied by PDP test in 3.5% NaCl solution. The curve for all the samples is shown in Figure 20. Higher E_{corr} and low i_{corr} values signify higher corrosion resistance. PDP tests were conducted to see the tendency of the coating to passivity. Two types of passive film form on the surface of the metal in an electrolyte: (i) one-dimensional absorptive film and (ii) three-dimensional solid film. If the compact and well-covered film is formed on the surface of the electrolyte by an electrochemical reaction, that can protect the corrosion completely. If the one-dimensional absorptive film of O_2 forms on the surface of the metal that can protect the dissolution of metal but not protect from corrosion completely.

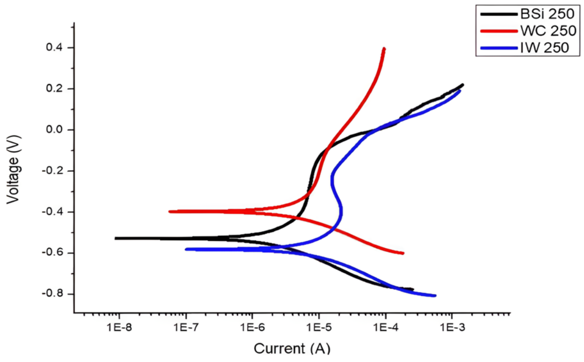

Figure 20. Tafel graph for all the coatings after 250 hr.

In the case of WC-10Co-4Cr coating chlorine ions corrode locally at the pores and carbide binder interface. The electrolyte penetrates into the pores of the coating removes the oxide layer and triggers the pitting corrosion. Porosities are preferred corrosion initiation sites; thus, the corrosion resistance of coating mainly depends upon the porosity. Another corrosion mechanism can be the formation of a micro-galvanic cell between the WC particle and the CoCr matrix as in the case of WC-10Co-4Cr coating, in which the WC particles act as cathode and CoCr matrix act as the anode as evident from the large cathodic to anodic reaction rate, corrosion is very high [16,17]. The presence of Cr improves the corrosion resistance of the coating by forming a Cr_2O_3 layer on the surface. Due to the presence of such passive film outside the pores, the corrosion potential inside the pore is lower compared to outside the pores. All the Coatings shown in Figure 20, form a passivation layer (probably Cr_2O_3 layer) on the surface which is characterized by the formation of a thin film that prevents the surface from charge transfer and, as a result, corrosion. In anodic polarization, this passive film breaks owing to an increase in current density at a certain potential (breakdown potential). Breakdown potential (~ 0 V for all the coatings) represents the breaking of the passive layer near the defects, triggering pitting corrosion. Corrosion resistance of the coating is mainly indicated by the value of E_{corr} as shown in Table 7. Maximum corrosion resistance occurs after 250 hr of immersion in electrolyte because of the formation of corrosion on the defects which again improves the corrosion resistance of the coating. The E_{corr} and i_{corr} value shown in Table 7 again indicates that the corrosion resistance of the coatings increases in the order of NiCrBSi > WC-10Co$_4$Cr > NiCrIW. The PDP results again support the EIS results, confirming that the corrosion resistance of the coatings are in the order of NiCrBSi > WC-10Co-4Cr > NiCrIW.

Table 7. E_{corr} (V) and i_{corr} (A/cm²) values for all types of coating.

Sample	E_{corr} (V)	i_{corr} (A/cm²)
WC-10Co-4Cr	-0.396	8×10^{-7}
NiCrBSi	-0.527	2.54×10^{-7}
NiCrIW	-0.580	1.97×10^{-6}

Conclusions

The detailed microstructural characterization and corrosion behavior of HVOF-coated WC-10Co-4Cr, NiCrBSi, and NiCrIW coatings have led to the following conclusions. The microstructure of WC-10Co-4Cr coatings shows a very large amount of semi-molten particles, and very little porosity (< 1.75% for an average thickness of 122 µm) which are not interconnected. WC-10Co-4Cr coating and NiCrIW coating are completely crystalline but NiCrBSi is amorphous in nature. The amorphous structure is because of the high melting point of the NiCrBSi powder approximately (1025 °C approximately) coupled with high combustion temperature and very high cooling rate of HVOF. The melting point decreases because of the presence of the boron (B). The microstructure of the NiCrBSi reveals that all the particles are completely melted during the HVOF coating process. NiCrBSi coating has the largest porosity (<2.36%) but porosities are not interconnected; the thickness of the NiCrBSi coating is approximately 77.8 µm. The Microstructure of NiCrIW has a very large amount of semi-molten particles, and a very small amount of porosity <1.75% but porosities are interconnected which is clearly visible on the microstructure and the average thickness is 56 µm.

Electrochemical impendence spectroscopy is very effective in studying the kinetics of the porous electrodes and the corrosion behavior of the coatings. Porosities and carbide matrix interface are preferred corrosion initiation sites, corrosion resistance of coating is mainly based upon the porosity for all types of coatings. Porosities are more dangerous if they are interconnected which we observe in the case of NiCrIW coating. The corrosion behavior of the WC-10Co-4Cr was very complicated as corrosion resistance of the coating decreases with increasing exposure time and corrosion starts after 12 hr (nearly 36hr) of immersion but after some time it again increases which is most probably because of accumulation of corrosion products near the defects. Whereas, corrosion resistance of the NiCrBSi coating decreases with increasing exposure time and corrosion starts after 102 hr (near to 200 hr) of immersion but after 250 hr it again increases which is most probably because of accumulation of corrosion products near the defects. Similarly, the corrosion resistance of NiCrIW coating decreases with increasing exposure time and corrosion starts after just immersion in immersion but after some time it again increases which is most probably because of the accumulation of

https://doi.org/10.61577/jcti.2023.100004

corrosion products near the defects. Potentiodynamic polarization test (PDP) was conducted after 250 hr of immersion result shows that the corrosion resistance of the coating is in the order of NiCrBSi > WC-10Co-4Cr > NiCrIW which is the same as EIS result.

Disclosure statement

No potential conflict of interest was reported by the authors.

References

1. Chawla V, Chawla A, Puri D, Prakash S, Gurbuxani PG, Sidhu BS. Hot Corrosion & Erosion Problems in Coal Based Power Plants in India and Possible Solutions - A Review. J Miner Mater Charact Eng. 2011;10:367-386.
2. Sidhu TS, Prakash S, Agrawal RD. Characterisations of HVOF sprayed NiCrBSi coatings on Ni- and Fe-based superalloys and evaluation of cyclic oxidation behaviour of some Ni-based superalloys in molten salt environment. Thin Solid Films. 2006;515:95-105.
3. Sidhu TS, Prakash S, Agrawal RD. Studies on the properties of high-velocity oxy-fuel thermal spray coatings for higher temperature applications. Mater Sci. 2005;41:805-823.
4. Saenger R, Martin D, Gabrielli C. Electrochemical characterization of plasma sprayed WC–Co coatings by impedance techniques. Surf Coatings Technol. 2005;194:335-343.
5. Bunshah RF. Handbook of Hard Coatings. 1st ed. USA: Noyes Publications; 2001. 1pp-535pp.
6. Lech Pawlowski, Thermal Spraying Techniques, In book: The Science and Engineering of Thermal Spray Coatings, Second Edition, 2008.
7. Guilemany JM, Fernández J, De Paco JM, Sanchez J. Corrosion resistance of HVOF WC-Co and TiC/Ni-Ti coatings sprayed on commercial steel. Surf Eng. 1998;14:133-135.
8. Gu P, Arsenault B, Beaudoin JJ, Legoux JG, Harvey B, Fournier J. Polarization Resistance of Stainless Steel-Coated Rebars. Cem Concr Res. 1998;28:321-327.
9. Pawlowski L. Properties of Coatings. 2nd ed. France: John Wiley & Sons; 2008. 383pp-541pp.
10. Kumar R, Kumar R, Kumar S. Erosion Corrosion Study of HVOF Sprayed Thermal Sprayed Coatings on Boiler Tubes: A Review. Int J Sci Manag Stud. 2018;1:1-6.
11. Souza VAD, Neville A. Corrosion and synergy in a WC-Co-Cr HVOF thermal spray coating-Understanding their role in erosion-corrosion degradation. Wear. 2005;259:171-180.
12. García J, Collado Ciprés V, Blomqvist A, Kaplan B. Cemented carbide microstructures: A review. Int J Refract Met Hard Mater. 2019;80:40-68.
13. Colin E, Leaute M, Roger T, Le Maguer A, Pawlowski L, Janssen J, et al. Microstructure investigation of HVOF sprayed WC-Co (Cr) coatings. Therm Spray Conf Proc. 2002; pp.858-862.
14. Staia MH, Carrasquero E. Wear behaviour of HVOF thermally sprayed WC-14Co-3Cr coatings. Surf Eng. 2000;16:515-518.
15. Perry JM, Neville A, Hodgkiess T. A comparison of the corrosion behavior of WC-Co-Cr and WC-Co HVOF thermally sprayed coatings by in situ Atomic Force Microscopy (AFM). J Therm Spray Technol. 2002;11:536-541.
16. Sherif ESM, El Rayes MM, Abdo HS. WC-Co and WC-Co-Cr coatings for the protection of API pipeline steel from corrosion in 4% NaCl solution. Coatings. 2020;10(3):275.
17. Vashishtha N, Khatirkar RK, Sapate SG. Tribological behaviour of HVOF sprayed WC-12Co, WC-10Co-4Cr and Cr3C2–25NiCr coatings. Tribol Int. 2017;105:55-68.
18. Zhao WM, Wang Y, Han T, Wu KY, Xue J. Electrochemical evaluation of corrosion resistance of NiCrBSi coatings deposited by HVOF. Surf Coatings Technol. 2004;183:118-125.
19. Otsubo F, Era H, Kishitake K. Structure and phases in nickel-base self-fluxing alloy coating containing high chromium and boron. J Therm Spray Technol. 2000;9:107-113.
20. Niranatlumpong P, Koiprasert H. The effect of Mo content in plasma-sprayed Mo-NiCrBSi coating on the tribological behavior. Surf Coatings Technol. 2010;205:483-489.
21. Zhang ZQ, Wang HD, Xu BS, Zhang GS. Characterization of microstructure and rolling contact fatigue performance of NiCrBSi/WC-Ni composite coatings prepared by plasma spraying. Surf Coatings Technol. 2015;261:60-68.
22. Chen J, Dong Y, Wan L, Yang Y, Chu Z, Zhang J, et al. Effect of induction remelting on the microstructure and properties of in situ TiN-reinforced NiCrBSi composite coatings. Surf Coatings Technol. 2018;340:159-166.
23. Human AM, Roebuck B, Exner H. Electrochemical polarisation and corrosion behaviour of cobalt and Co(W,C) alloys in 1 N sulphuric acid. Mater Sci Eng A. 1998;241:202-210.
24. Méndez-Medrano KO, Martínez-González CJ, Alvarado-Hernández F, Jiménez O, Baltazar-Hernández VH, Ruiz-Luna H. Microstructure and Properties Characterization of WC-Co-Cr Thermal Spray Coatings. J Miner Mater Charact Eng. 2018;06:482-497.
25. Magnani M, Suegama PH, Espallargas N, Dosta S, Fugivara CS, Guilemany JM, et al. Influence of HVOF parameters on the corrosion and wear resistance of WC-Co coatings sprayed on AA7050 T7. Surf Coatings Technol. 2008;202:4746-4757.
26. Liu C, Leyland A, Lyon S, Matthews A. Electrochemical impedance spectroscopy of PVD-TiN coatings on mild steel and AISI316 substrates. Surf Coatings Technol. 1995;76:615-622.
27. Xiao JK, Wu YQ, Zhang W, Chen J, Wei XL, Zhang C. Microstructure, wear and corrosion behaviors of plasma sprayed NiCrBSi-Zr coating. Surf Coatings Technol. 2019;360:172-180.
28. Brad AJ, Faulkner LR. Electrochemical Methods: Fundamentals and Applications. John Wiley and Sons. 2001.
29. Verdian MM, Raeissi K, Salehi M. Electrochemical impedance spectroscopy of HVOF-sprayed NiTi intermetallic coatings deposited on AISI 1045 steel. J Alloys Compd. 2010;507:42-46.
30. Verdian MM, Raeissi K, Salehi M. Corrosion performance of HVOF and APS thermally sprayed NiTi intermetallic coatings in 3.5% NaCl solution. Corros Sci. 2010;52:1052-1059.

https://doi.org/10.61577/jcti.2023.100004